Ideal diode equation for organic heterojunctions. I. Derivation and application

N. C. Giebink,[1,2,3] G. P. Wiederrecht,[2,3] M. R. Wasielewski,[2,3,4] and S. R. Forrest[1,*]
[1]*Departments of Electrical Engineering, Materials Science, and Physics, University of Michigan, Ann Arbor, Michigan 48109, USA*
[2]*Center for Nanoscale Materials, Argonne National Laboratory, Argonne, Illinois 60439, USA*
[3]*Argonne-Northwestern Solar Energy Research Center (ANSER), Northwestern University, Evanston, Illinois 60208, USA*
[4]*Department of Chemistry, Northwestern University, Evanston, Illinois 60208, USA*
(Received 4 May 2010; revised manuscript received 4 August 2010; published 4 October 2010)

The current-voltage characteristics of organic heterojunctions (HJs) are often modeled using the generalized Shockley equation derived for inorganic diodes. However, since this description does not rigorously apply to organic semiconductor donor-acceptor (D-A) HJs, the extracted parameters lack a clear physical meaning. Here, we derive the current density-voltage (*J-V*) characteristic specifically for D-A HJ solar cells and show that it predicts the general dependence of dark current, open-circuit voltage (V_{oc}), and short-circuit current (J_{sc}) on temperature and light intensity as well as the maximum V_{oc} for a given D-A material pair. We propose that trap-limited recombination due to disorder at the D-A interface leads to the introduction of two temperature-dependent ideality factors and show that this describes the dark current of copper phthalocyanine/C_{60} and boron subphthalocyanine/C_{60} cells at low temperature, where fits to the generalized Shockley equation break down. We identify the polaron pair recombination rate as a key factor that determines the *J-V* characteristics in the dark and under illumination and provide direct measurements of this process in our companion paper II [N. C. Giebink, B. E. Lassiter, G. P. Wiederrecht, M. R. Wasielewski, and S. R. Forrest, Phys. Rev. B **82**, 155306 (2010)]. These results provide a general physical framework for interpreting the *J-V* characteristics and understanding the efficiency of both small molecule and polymer organic, planar and bulk HJ solar cells.

DOI: 10.1103/PhysRevB.82.155305 PACS number(s): 72.20.Jv, 72.80.Le, 73.61.Ph, 73.50.Gr

I. INTRODUCTION

The current density vs voltage (*J-V*) characteristics of organic semiconductor heterojunctions are often similar to those of inorganic *p-n* junctions. As a consequence, theoretical treatments based on the generalized Shockley equation[1,2] originally derived for inorganic devices, have been extended to model the operation of organic solar cells.[3–6] This phenomenological approach often yields a reasonably accurate description, although it fails in some cases and obscures the inherently different physics of organic semiconductors whose understanding would lead to a richer, more rigorous picture of these structures. In particular, the Shockley equation is derived for inorganic *p-n* junctions with well-developed energy-band structure where thermal and optical excitation results in delocalized free charge carriers. In contrast, organic semiconductors are generally characterized by hopping transport and tightly bound, localized exciton states that require significant energy to dissociate into free charge carriers.

Here, we derive the ideal diode equation specifically for the case of organic heterojunctions (HJs). Explicitly treating polaron pair generation, recombination and dissociation at the HJ, we develop a current-voltage characteristic similar in form to the Shockley equation[7] but differing in several key aspects. In particular, it predicts the temperature dependence of the dark current, the intensity and temperature dependence of the open-circuit voltage (V_{oc}) and short-circuit current (J_{sc}), and the maximum V_{oc} attainable for a given small molecule or polymer HJ material pair. Additionally, we propose that the diode ideality factor arises from recombination via disorder-induced traps at the heterointerface, and analytically treat the case in which these traps have an exponential energetic distribution extending into the energy gap between the highest occupied (HOMO) and lowest unoccupied molecular orbitals (LUMO). The model is applied to data obtained for two archetype, planar HJ organic photovoltaic cells composed of copper phthalocyanine (CuPc) and boron subphthalocyanine chloride (SubPc) donors and a fullerene (C_{60}) acceptor.

This paper is organized as follows. Section II details our theoretical approach and derivation of the ideal organic heterojunction diode equation for both the trap-free case and that involving an exponential trap distribution. Experimental methods are given in Sec. III, and model results along with device data for CuPc/C_{60} and SubPc/C_{60} cells are presented in Sec. IV. In Sec. V, we evaluate the model within the context of the data and discuss its implications for organic solar cell efficiency. Conclusions are presented in Sec. VI. In the companion paper II,[8] we provide direct experimental support for our physical assumptions by presenting observations of polaron recombination dynamics at these heterojunctions.

II. THEORY

A. Current-voltage characteristics in the absence of traps

Our treatment assumes that current is governed solely by generation and recombination at the heterojunction and that both processes proceed through the polaron pair (PP) intermediate state. The average polaron pair separation, a_0, thus defines the "volume" of the heterojunction region, as shown in Fig. 1(a). Current outside of this region is unipolar with pure hole and electron currents flowing in the donor and acceptor bulk, respectively.

The schematic in Fig. 1(a) also defines the energetics, where the interfacial gap, ΔE_{HL}, is the difference between

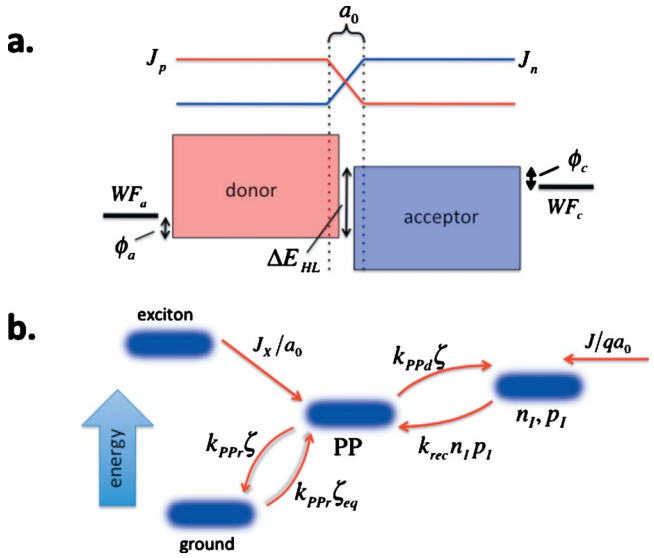

FIG. 1. (Color online) (a) Energy-level diagram showing the anode and cathode work functions, WF_a and WF_c, and their associated injection barriers ϕ_a and ϕ_c, respectively. The interfacial gap, ΔE_{HL}, is the energy difference between the highest occupied molecular orbital energy of the donor and the lowest unoccupied molecular orbital energy of the acceptor. Current is unipolar in the donor (J_p) and acceptor (J_n) layers and is determined from generation/recombination in the HJ region, roughly defined by the spatial extent, a_0, of the polaron pair distribution at the interface. (b) Processes occurring within the HJ region. Excitons diffuse, with current density, J_X, to the HJ and undergo charge transfer to form polaron pairs. These may recombine, at rate k_{PPr}, or dissociate with rate, k_{PPd}, as determined by the Onsager-Braun model (Ref. 10). The current density, J, contributes to the interfacial free electron (n_I) and hole (p_I) densities, which bimolecularly recombine to form polaron pairs at rate k_{rec}.

donor HOMO and acceptor LUMO along with any shift due to formation of an interface dipole. The hole and electron injection barriers at the anode and cathode are ϕ_a and ϕ_c, respectively, again including any interface dipoles, and the built-in potential of the device is given by the corresponding difference in contact work functions: $V_{bi}=WF_a-WF_c$.

Figure 1(b) shows the processes that occur within the HJ volume. The recombination of polaron pairs is described via

$$\frac{J_X}{a_0} - k_{\mathrm{PP}r}(\zeta - \zeta_{eq}) - k_{\mathrm{PP}d}\zeta + k_{rec}n_I p_I = 0, \tag{1}$$

and for free carriers:

$$k_{\mathrm{PP}d}\zeta - k_{rec}n_I p_I + \frac{J}{qa_0} = 0, \tag{2}$$

where steady-state conditions are assumed. Here, ζ is the PP density, J_X is the exciton current density diffusing to the interface, J is the charge current density flowing through the device, q is the electron charge, and n_I and p_I are the interfacial free electron and hole densities, respectively. Definitions of important variables used in this section are summarized in Table I.

Polaron pairs recombine to the ground state at rate $k_{\mathrm{PP}r}$, which is also linked to the thermal equilibrium PP population, ζ_{eq}, determined by detailed balance.[9] Polaron pairs dissociate at rate $k_{\mathrm{PP}d}$, which is a function of temperature and the electric field at the interface according to the Onsager-Braun model[10] (see Appendix). Finally, free carriers bimolecularly recombine to form PPs with rate constant, k_{rec}, approximated by its bulk Langevin value, $q\mu_{tot}/\varepsilon$.[11,12] Here, μ_{tot} is the sum of the electron and hole mobilities in the acceptor and donor layers, respectively, and ε is the average permittivity.

Solving Eq. (1) for the PP density and substituting the result into Eq. (2) gives

$$J = qa_0k_{rec}\left(\frac{k_{\mathrm{PP}r}}{k_{\mathrm{PP}d}+k_{\mathrm{PP}r}}\right)\left(n_I p_I - \frac{k_{\mathrm{PP}d}}{k_{\mathrm{PP}d,eq}}n_{I,eq}p_{I,eq}\right) - qJ_X\left(\frac{k_{\mathrm{PP}d}}{k_{\mathrm{PP}d}+k_{\mathrm{PP}r}}\right), \tag{3}$$

where we have used $\zeta_{eq}=k_{rec}n_{I,eq}p_{I,eq}/k_{\mathrm{PP}d,eq}$ from Eq. (2). The subscript eq indicates the thermal equilibrium value in the absence of bias or illumination. Similar to the Shockley equation, we assume quasi-equilibrium. Hence, the carrier densities at the interface (n_I,p_I) and contacts (n_C,p_C) are related via[7]

$$n_I = n_C \exp\left[\frac{\delta_{\mathrm{A}}q(V_a - V_{bi})}{k_bT}\right] \tag{4a}$$

and

$$p_I = p_C \exp\left[\frac{\delta_{\mathrm{D}}q(V_a - V_{bi})}{k_bT}\right], \tag{4b}$$

where $\delta_{\mathrm{D}}+\delta_{\mathrm{A}}=1$ are the fractions of the potential dropped across the donor (D) and acceptor (A) layers, respectively. Here, V_a is the applied bias, k_b is Boltzmann's constant, and T is the temperature. These relations are strictly valid only when $J=0$, but are a good approximation at low current when J is much smaller than either of its drift or diffusion components.

Use of Eq. (4) in Eq. (3) yields

$$J = qa_0k_{rec}n_Cp_C(1-\eta_{\mathrm{PP}d})\exp(-qV_{bi}/k_bT) \times\left\{\exp(qV_a/k_bT) - \frac{k_{\mathrm{PP}d}}{k_{\mathrm{PP}d,eq}}\right\} - q\eta_{\mathrm{PP}d}J_X, \tag{5}$$

where $\eta_{\mathrm{PP}d}=k_{\mathrm{PP}d}/(k_{\mathrm{PP}d}+k_{\mathrm{PP}r})$ is the PP dissociation probability.[10,13] Assuming detailed balance of the charge density adjacent to an injecting contact,[14] we write

$$n_C = f(F_c,T)N_{\mathrm{LUMO}}\exp(-\phi_c/k_bT), \tag{6}$$

where N_{LUMO} is the density of states (DOS) at the acceptor LUMO and F_c is the electric field at the cathode contact. The analogous relation involving the injection barrier, ϕ_a, [see Fig. 1(a)] exists for holes at the anode with N_{HOMO} as the DOS at the donor HOMO. The term, $f(F_c,T)$ is dominated by Schottky barrier lowering; since it is near unity except for the case of high field and/or low temperature, we neglect it

TABLE I. Definition of variables.

Variable	Definition	Units
	Trap-free	
J_X	Exciton current density reaching the HJ	$cm^{-2}\ s^{-1}$
ζ	Polaron pair density at the HJ	cm^{-3}
a_0	Polaron pair spatial extent	cm
k_{rec}	Free carrier bimolecular recombination coefficient	$cm^3\ s^{-1}$
$k_{\mathrm{PP}d}$	Polaron pair dissociation rate	s^{-1}
$k_{\mathrm{PP}r}$	Polaron pair recombination rate	s^{-1}
$\eta_{\mathrm{PP}d}$	Polaron pair dissociation efficiency	
$\delta_{\mathrm{A}}, \delta_{\mathrm{D}}$	Fractions of the potential dropped across acceptor and donor layers	
n_I, p_I	Free electron and hole densities at the HJ interface	cm^{-3}
n_C, p_C	Free electron and hole densities adjacent to respective contacts	cm^{-3}
$N_{\mathrm{HOMO}}, N_{\mathrm{LUMO}}$	Donor HOMO and acceptor LUMO edge densities of states	cm^{-3}
	Exponential trap distribution	
n_{It}, p_{It}	Trapped free electron and hole densities at the HJ interface	cm^{-3}
$T_{t,\mathrm{D}}, T_{t,\mathrm{A}}$	Characteristic temperatures for hole and electron trap distributions in the donor and acceptor	K
$H_{\mathrm{D}}, H_{\mathrm{A}}$	Band-edge trap densities in the donor and acceptor	cm^{-3}
$k_{rec,n}, k_{rec,p}$	Recombination coefficients for recombination of free electrons with trapped holes and vice versa	$cm^3\ s^{-1}$
$n_{\mathrm{D}}, n_{\mathrm{A}}$	Ideality factors due to trap-limited recombination in the donor and acceptor	

here. Thus we arrive at the ideal diode equation for an organic HJ in the absence of traps

$$J = qa_0 k_{rec} N_{\mathrm{HOMO}} N_{\mathrm{LUMO}} (1 - \eta_{\mathrm{PP}d}) \exp(-\Delta E_{HL}/k_b T) \times \left\{ \exp(qV_a/k_b T) - \frac{k_{\mathrm{PP}d}}{k_{\mathrm{PP}d,eq}} \right\} - q\eta_{\mathrm{PP}d} J_X = J_{s0} \left\{ \exp(qV_a/k_b T) - \frac{k_{\mathrm{PP}d}}{k_{\mathrm{PP}d,eq}} \right\} - q\eta_{\mathrm{PP}d} J_X, \quad (7)$$

where $\Delta E_{HL} = \phi_a + \phi_c + qV_{bi}$ from Fig. 1(a). Note that this equation carries an implicit dependence on temperature and the interfacial electric field through $k_{\mathrm{PP}d}(F_I, T)$, and consequently $\eta_{\mathrm{PP}d}$; the solution for these terms is provided in the Appendix.

In the absence of illumination ($J_X = 0$), Eq. (7) represents the ideal organic HJ current density-voltage relationship. Compared to the Shockley equation, the prefactor of the bracketed term is analogous to the dark saturation current (called J_{s0} here), whose temperature dependence is predominantly exponential in ΔE_{HL}.[7] For $V_a < 0$, the interfacial field is high and aids dissociation. Thus, $k_{\mathrm{PP}d}$ grows larger than $k_{\mathrm{PP}d,eq}$ and the reverse saturation current increases with increasing reverse bias, as typically observed in organic HJs.[4,6]

Under forward bias, $k_{\mathrm{PP}d}$ is similar to or less than $k_{\mathrm{PP}d,eq}$ and the current density increases exponentially with an ideality factor $n = 1$. In this case, Eq. (7) reduces to the familiar

$$J = J_{s0}\{\exp(qV_a/k_b T) - 1\} - q\eta_{\mathrm{PP}d} J_X \quad (8)$$

frequently used to model organic HJ solar cells. As expected, the photocurrent (last term on the right) is directly proportional to the PP dissociation efficiency, which diminishes with increasing forward bias.

Solving Eq. (7) for the open-circuit voltage gives

$$qV_{oc} = \Delta E_{HL} - k_b T \ln\left[\left(\frac{k_{\mathrm{PP}r}}{k_{\mathrm{PP}d}} \right) \frac{k_{rec} N_{\mathrm{HOMO}} N_{\mathrm{LUMO}}}{J_X/a_0} \right]. \quad (9)$$

Equation (9) predicts that V_{oc} should increase with decreasing temperature and that it should increase as the logarithm of J_X (proportional to intensity) with slope $k_b T/q$. When polaron pairs are strongly coupled to the ground state, $k_{\mathrm{PP}r}$ is large and V_{oc} decreases. At V_{oc}, the interfacial field, F_I, is small or even reverses direction (i.e., aiding recombination). In this case, $k_{\mathrm{PP}d}$ takes on its zero-field value, $k_{\mathrm{PP}d} \approx [3k_{rec}/4\pi a_0^3]\exp(-E_B/k_b T)$, where E_B is the polaron pair binding energy.[10,11] Recognizing $4\pi a_0^3/3$ as the volume oc-

cupied by a polaron pair, this relationship may be inserted into Eq. (9) to give

$$qV_{oc} = (\Delta E_{HL} - E_B) - k_b T \ln\left[\frac{k_{\mathrm{PP}r} N_{\mathrm{HOMO}} N_{\mathrm{LUMO}}}{\zeta_{\max} J_X / a_0}\right], \quad (10)$$

where $\zeta_{\max}$ is the maximum PP density that can be sustained at the interface (i.e., all states are occupied).

According to Eq. (10), the maximum possible open-circuit voltage, $V_{oc}^{\max}$, is equal to the interfacial energy gap, less the polaron pair binding energy. This expression is analogous to those previously suggested by Rand *et al.*,[5] Cheyns *et al.*,[15] and Vandewal *et al.*[16] and is also consistent with the experimental results of Rand. The maximum open-circuit voltage is reached in the limit $T \to 0$ or when J_X increases to $J_X = a_0 k_{\mathrm{PP}r} N_{\mathrm{HOMO}} N_{\mathrm{LUMO}} / \zeta_{\max}$. Since $\zeta_{\max} \sim N_{\mathrm{HOMO}} \sim N_{\mathrm{LUMO}}$ are all on the order of the molecular density, this final condition becomes $J_X = a_0 k_{\mathrm{PP}r} N_{\mathrm{HOMO}}$, which states that the exciton current is delivering the maximum density of charge that recombination at the interface can sustain. It is not possible to increase J_X beyond this limit since, with all PP states occupied, any additional excitons reaching the interface cannot be dissociated. Equation (10) may be viewed as an organic analog to the band-gap limitation of $V_{oc}^{\max}$ in inorganic solar cells established by Shockley and Queisser.[17]

B. Current-voltage characteristics in the presence of an exponential trap distribution

Most organic solar cells are characterized by significant molecular disorder in both the donor and acceptor layers, leading to a broad density of states with an approximately Gaussian energetic distribution at the HOMO and LUMO levels.[18–20] Evidence also suggests that ground-state interactions between the donor and acceptor further broaden this distribution near the HJ interface.[21,22] The low-energy tail of the DOS, where most charge carriers reside, can be modeled as an exponential distribution of traps.[11,20,23] This changes the kinetics of recombination at the interface and introduces an ideality factor $n > 1$ in the diode equation, as shown below.

Assuming an exponential trap distribution with characteristic trap temperature, $T_{t,\mathrm{A}}$, in the acceptor, the trapped (n_t) and free (n) electron densities are related approximately via[11,23]

$$n_t \approx H_{\mathrm{A}} \exp\left(\frac{E_{Fn} - E_{\mathrm{LUMO}}}{k_b T_{t,\mathrm{A}}}\right) \approx H_{\mathrm{A}} \left(\frac{n}{N_{\mathrm{LUMO}}}\right)^{1/l_{\mathrm{A}}}, \quad (11)$$

where H_{A} is the density of trap states at the acceptor LUMO, E_{Fn} is its electron quasi-Fermi energy, E_{LUMO} is the LUMO energy of the acceptor, and $l_{\mathrm{A}} = T_{t,\mathrm{A}}/T$. A similar relationship holds for the trapped hole density, p_t, in the donor. Assuming that the trapped carrier density significantly exceeds the free carrier density, Eq. (3) becomes

$$J = qa_0 \left(\frac{k_{\mathrm{PP}r}}{k_{\mathrm{PP}d} + k_{\mathrm{PP}r}}\right) \left\{ k_{rec,n} \left(n_I p_{It} - \frac{k_{\mathrm{PP}d}}{k_{\mathrm{PP}d,eq}} n_{I,eq} p_{It,eq} \right) + k_{rec,p} \left(p_I n_{It} - \frac{k_{\mathrm{PP}d}}{k_{\mathrm{PP}d,eq}} p_{I,eq} p_{It,eq} \right) \right\} - qJ_X \left(\frac{k_{\mathrm{PP}d}}{k_{\mathrm{PP}d} + k_{\mathrm{PP}r}} \right), \quad (12)$$

where recombination now occurs primarily at trap states and $k_{rec,n}$ and $k_{rec,p}$ are the rate constants describing recombination at the HJ between a free electron in the acceptor (n_I) with a trapped hole in the donor (p_{It}), and vice versa.

Using Eqs. (4), (11), and (12) gives

$$J = qa_0(1 - \eta_{\mathrm{PP}d}) \left\{ k_{rec,n} N_{\mathrm{LUMO}} H_{\mathrm{D}} \exp(-\alpha_{\mathrm{D}}/k_b T) \times \left[\exp(qV_a/n_{\mathrm{D}} k_b T) - \frac{k_{\mathrm{PP}d}}{k_{\mathrm{PP}d,eq}} \right] + k_{rec,p} N_{\mathrm{HOMO}} H_{\mathrm{A}} \times \exp(-\alpha_{\mathrm{A}}/k_b T) \left[\exp(qV_a/n_{\mathrm{A}} k_b T) - \frac{k_{\mathrm{PP}d}}{k_{\mathrm{PP}d,eq}} \right] \right\} - q\eta_{\mathrm{PP}d} J_X, \quad (13a)$$

where

$$\alpha_{\mathrm{D}} = \frac{\Delta E_{HL}}{n_{\mathrm{D}}} + \frac{l_{\mathrm{D}} - 1}{l_{\mathrm{D}}} (\delta_{\mathrm{D}} \phi_c - \delta_{\mathrm{A}} \phi_a) \quad (13b)$$

and

$$\alpha_{\mathrm{A}} = \frac{\Delta E_{HL}}{n_{\mathrm{A}}} + \frac{l_{\mathrm{A}} - 1}{l_{\mathrm{A}}} (\delta_{\mathrm{A}} \phi_a - \delta_{\mathrm{D}} \phi_c). \quad (13c)$$

The ideality factors, n_{A} and n_{D} are given by

$$n_{\mathrm{A}} = \frac{l_{\mathrm{A}}}{\delta_{\mathrm{D}}(l_{\mathrm{A}} - 1) + 1} \quad (14a)$$

and

$$n_{\mathrm{D}} = \frac{l_{\mathrm{D}}}{\delta_{\mathrm{A}}(l_{\mathrm{D}} - 1) + 1}. \quad (14b)$$

More compactly, Eq. (13) becomes the ideal diode equation in the presence of traps

$$J = J_{s\mathrm{D}} \left[\exp(qV_a/n_{\mathrm{D}} k_b T) - \frac{k_{\mathrm{PP}d}}{k_{\mathrm{PP}d,eq}} \right] + J_{s\mathrm{A}} \left[\exp(qV_a/n_{\mathrm{A}} k_b T) - \frac{k_{\mathrm{PP}d}}{k_{\mathrm{PP}d,eq}} \right] - q\eta_{\mathrm{PP}d} J_X, \quad (15a)$$

which simplifies to

$$J = J_{s\mathrm{D}} [\exp(qV_a/n_{\mathrm{D}} k_b T) - 1] + J_{s\mathrm{A}} [\exp(qV_a/n_{\mathrm{A}} k_b T) - 1] - q\eta_{\mathrm{PP}d} J_X, \quad (15b)$$

when $k_{\mathrm{PP}d} \leq k_{\mathrm{PP}d,eq}$ under forward bias [cf. Eq. (8)]. Here $J_{s\mathrm{D}}$ and $J_{s\mathrm{A}}$ are the dark saturation currents given by the prefactors in Eq. (13). Thus, in general, there are two sources of dark current stemming from the recombination of free electrons with trapped holes and vice versa. Each pathway pro-

duces its own ideality factor (n_D and n_A, respectively) and dark saturation current, both of which depend on the balance of the voltage drop across the D and A layers as well as their characteristic trap temperatures.

In the case of a perfectly symmetric device, with identical transport properties and injection barriers for electrons and holes, Eq. (13) simplifies to

$$J = qa_0(1-\eta_{PPd})2k_{rec,sym}N_{sym}H_{sym}\exp(-\Delta E_{HL}/n_{sym}k_bT) \times\left\{\exp(qV_a/n_{sym}k_bT) - \frac{k_{PPd}}{k_{PPd,eq}}\right\} - q\eta_{PPd}J_X \quad (16a)$$

or

$$J = J_{sym}\{\exp(qV_a/n_{sym}k_bT) - 1\} - q\eta_{PPd}J_X, \quad (16b)$$

where $n_{sym}=2l_{sym}/(l_{sym}+1)$ and the subscript *sym* indicates parameters that are equivalent for holes in the donor and electrons in the acceptor. Solving for V_{oc} leads to

$$qV_{oc} = \Delta E_{HL} - n_{sym}k_bT\ln\left[\left(\frac{k_{PPr}}{k_{PPd}}\right)\frac{k_{rec,sym}N_{sym}^2}{J_X/a_0}\right], \quad (17)$$

resulting in a slope of $n_{sym}k_bT/q$ when plotted versus the logarithm of intensity. The maximum open-circuit voltage, V_{oc}^{max}, still reduces to $\Delta E_{HL}-E_B$, since in the limit of high light intensity, the original assumption of $n_t, p_t \gg n, p$ no longer holds. In this regime all traps are filled and recombination is no longer trap limited, hence, Eq. (17) reverts to Eq. (9).

Figure 2(a) shows a set of dark *J*-*V* characteristics calculated using Eq. (13) over the temperature range from 120 to 296 K for a device using the parameters listed in Table II, which are typical of organic photovoltaic cells. We have included a series resistance of $R_s=1\ \Omega\ \mathrm{cm}^2$ (in which case, V_a is replaced by V_a-JR_s) and assumed that most of the potential is dropped across the donor layer, resulting in different ideality factors according to Eq. (14). The ideality factors and their associated dark saturation currents are given in Fig. 2(b). Both ideality factors increase with decreasing temperature, and the quantity $n\ln(J_s)$, where the argument in the logarithm is implicitly normalized[5] to 1 $\mathrm{A/cm}^2$, is nonlinear when plotted vs $1/k_bT$. This contrasts with previous analyses based on the Shockley equation,[5,24] which predict a linear relationship for this quantity with a slope equal to $-\Delta E_{HL}/2$.

In comparison to the dark current characteristics of many reported planar HJ organic solar cells,[4–6] we make the following observations. In the generalized Shockley equation, increasing dark current with reverse bias is phenomenologically accounted for by a shunt resistance whereas here it is due to the field-dependent dissociation of thermally generated PPs [i.e., $k_{PPd}=k_{PPd}(F_I)$]. The two slopes routinely observed in semilog plots under forward bias[4–6] (the second is only evident at low temperature for some devices) are not the result of a shunt resistance and a single diode ideality factor, but rather of two ideality factors that reflect recombination with trapped carriers at each side of the HJ.

In forward bias, the ideality factor n_D is evident in the slope of the *J*-*V* characteristics for $0<V_a<0.3$ V whereas n_A dominates at $0.4<V_a<0.7$ V, beyond which series resistance from contacts and the layer bulk limits the current. The asymmetry of the voltage dropped across the donor and acceptor layers ($\delta_A=0.1$ is assumed here) is the primary cause of the difference in ideality factors and is expected by analogy to the asymmetries in organic light emitting devices.[25,26]

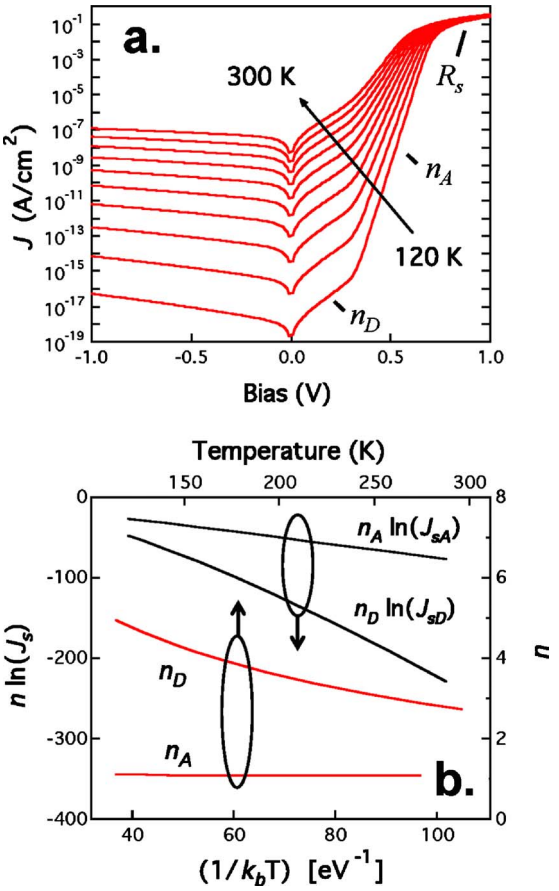

FIG. 2. (Color online) (a) Calculated dark current density (*J*)-voltage characteristics over the temperature range from 120 to 300 K in 20 K increments using Eq. (13) and the parameters in Table II. The slope in reverse bias is due to the field-dependent dissociation of thermally generated polaron pairs. In forward bias, three regions are apparent. At $V_a<0.3$ V, trap-limited recombination involving free acceptor electrons and trapped donor holes dominates, and the slope is proportional to the donor ideality factor, n_D. At higher bias, the inverse process dominates (i.e., free donor holes recombine with trapped acceptor electrons) and the slope is proportional to the acceptor ideality factor, n_A. Series resistance (R_s) limits the current at $V_a>0.8$ V. (b) Diode parameters *n* and $n\ln(J_s)$ corresponding to the dark currents in (a). Both ideality factors increase with decreasing temperature, though n_A does so only slightly.

At low bias, the current is predominantly mediated by PPs formed from the recombination of free holes in the donor with trapped electrons in the acceptor. At higher bias ($0.4<V_a<0.7$), the reverse process dominates, and the slope is determined by n_A. As temperature decreases, carriers freeze into the trap states that constitute the tail of the DOS, and recombination becomes further trap limited, resulting in the increase in both ideality factors with temperature [see Fig. 2(b), Eq. (14)]. The change is small for n_A, increasing from $n_A=1.07$ at room temperature to $n_A=1.10$ at $T=120$ K.

TABLE II. Model parameter values.

Parameter	Value
Donor thickness=acceptor thickness	40 nm
ΔE_{HL}	1.2 eV
V_{bi}	0.5 V
$T_{t,A}=T_{t,D}$	1000 K
$H_A=H_D$	10^{18} cm^{-3}
$N_{HOMO}=N_{LUMO}$	10^{21} cm^{-3}
δ_A	0.1
a_0	1.5 nm
k_{PPr}	1 μs^{-1}
$k_{rec,n}=k_{rec,p}=q\mu/\varepsilon$	$\varepsilon/\varepsilon_0=3$, $\mu=10^{-3}$ cm^2/V s
R_s	1 Ω cm^2

In Fig. 3(a), we calculate the intensity dependence of V_{oc}, J_{sc}, and the fill factor, FF, from Eq. (13), using the same parameters from the dark J-V characteristics of Fig. 2. The exciton current density, qJ_X, is directly proportional to light intensity and is approximately equal to J_{sc}. The FF increases and then saturates at high light intensity. The open-circuit voltage increases as the log of intensity with the slopes $n_D k_b T/q$ and $n_A k_b T/q$ at low and high intensities, respectively, as expected from the double exponential form of Eq. (13).

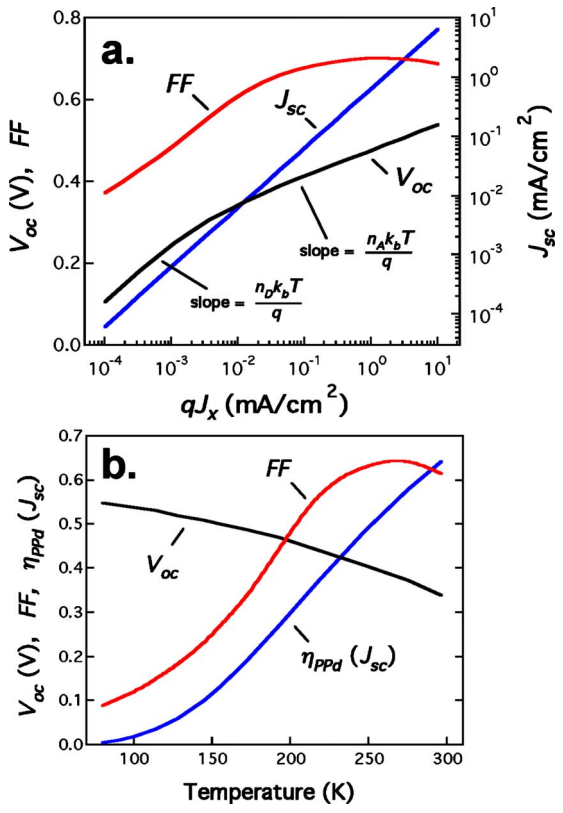

FIG. 3. (Color online) (a) Intensity dependence of the open-circuit voltage (V_{oc}), short-circuit current (J_{sc}), and FF derived from the same model and parameters as in Fig. 2. (b) Temperature dependence of V_{oc}, FF, and polaron pair dissociation efficiency at short circuit, $\eta_{PPd}(J_{sc})$.

Figure 3(b) shows the temperature dependence of V_{oc}, FF, and the polaron pair dissociation efficiency at short circuit, η_{PPd}. The open-circuit voltage increases by $\sim$0.25 V at low temperature, as compared to its value at $T=300$ K whereas FF steadily declines for $T \leq 200$ K. The polaron pair dissociation efficiency decreases substantially with decreasing T from its room temperature value of $\eta_{PPd} \sim 0.6$. The theoretical trends in Fig. 3 have been observed in both small molecular and polymer organic solar cells.[3,5,27–31]

III. EXPERIMENTAL METHODS

Conventional CuPc/C_{60} and SubPc/C_{60} cells were fabricated on glass substrates coated with a transparent indium-tin oxide (sheet resistance of $\sim$15 $\Omega/\square$) anode prepatterned into 1-mm-wide stripes. All organic materials were purified by thermal gradient sublimation prior to use. Following a thorough solvent degrease of the substrate,[20] layers were deposited sequentially by thermal evaporation in a chamber with base pressure $\sim 10^{-7}$ Torr. The devices consist of 20-nm-thick CuPc or 11-nm-thick SubPc, followed by 40-nm-thick C_{60}, 10-nm-thick bathocuprine, and a 100-nm-thick Al cathode, deposited through a shadow mask as 1 mm stripes positioned orthogonally to the patterned anode to form 1 mm^2 device areas.

Cell efficiency was characterized at room temperature in air under simulated AM1.5G illumination and found to be comparable to previously reported devices using these materials combinations.[24,32] Temperature-dependent measurements were conducted in an evacuated, closed-cycle He cryostat using illumination from the $\lambda=496$ nm line of an Ar^+ laser with an intensity of 30 mW/cm^2. The temperature of each device was measured with a Ge thermistor soldered to the substrate surface. Current-voltage characteristics were obtained using an Agilent 4156 semiconductor parameter analyzer at a voltage sweep rate of 0.2 V/s to minimize unwanted capacitive effects. The current-voltage characteristics were fit using a nonlinear least-squares trust-region algorithm with statistical weighting.

IV. RESULTS

In Figs. 4(a) and 4(b), the J-V data taken over a range of temperatures are fit for both CuPc/C_{60} and SubPc/C_{60} cells to the ideal diode equation of Eq. (15) modified to include the effect of series resistance, R_s

$$J = J_{sD}\{\exp[q(V_a - JR_s)/n_D k_b T] - 1\} + J_{sA}\{\exp[q(V_a - JR_s)/n_A k_b T] - 1\} - q\eta_{PPd} J_X. \quad (18)$$

The results of Eq. (18) match the data over the entire temperature range whereas those calculated using the generalized Shockley equation[5,7] and plotted in Figs. 4(c) and 4(d) show increasingly poor agreement at low temperature and voltage.

Figure 5 presents the ideality factors and dark saturation currents extracted from the fits in Figs. 4(a) and 4(b). Both sets of ideality factors increase with decreasing temperature, similar to the prediction of Fig. 2(b), although there is a discrepancy in their overall magnitude as discussed in Sec.

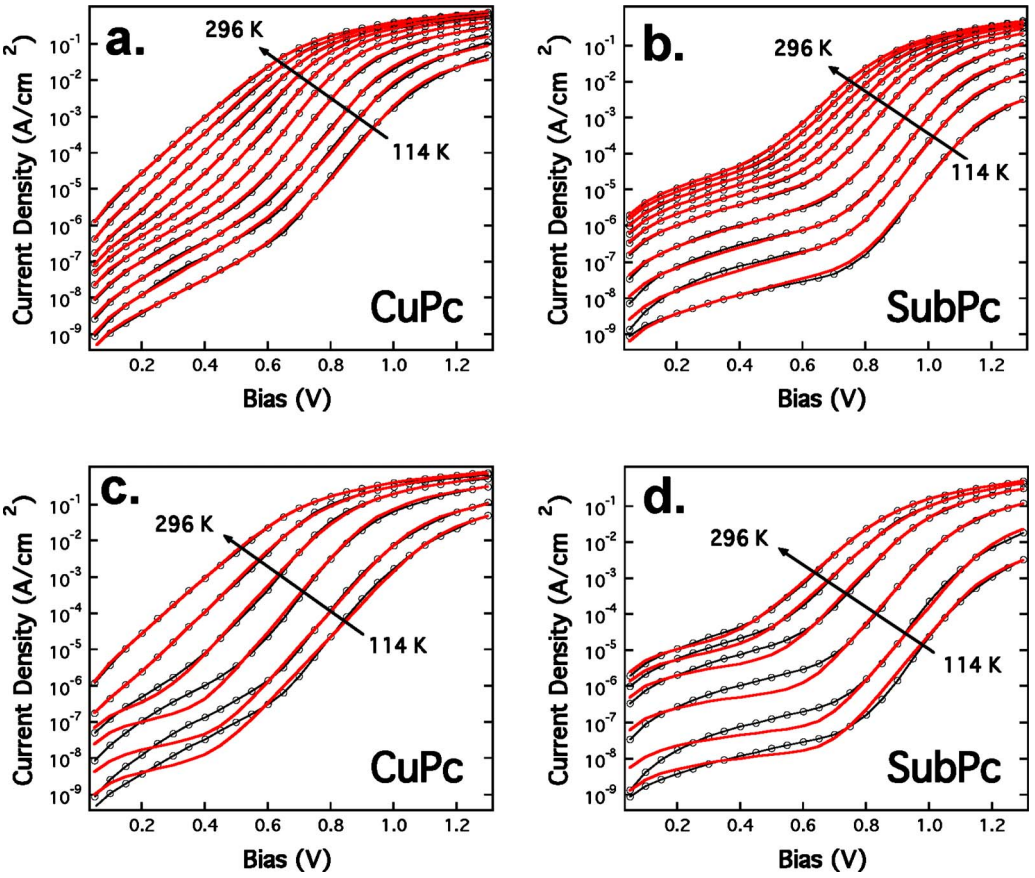

FIG. 4. (Color online) Dark current density vs forward voltage for (a) CuPc/C_{60} and (b) SubPc/C_{60} devices recorded for $T=296$, 275, 247, 218, 193, 171, 155, 145, 128, and 114 K. Bold (red) lines indicate fits to Eq. (18) in the text. Thin (black) lines connect the data points and serve as a guide to the eyes. Both data sets are refit using the generalized Shockley equation in (c) and (d), where the difference between data and theory is most pronounced at low voltage and temperature. Several intermediate temperatures have been omitted in (c) and (d) for clarity.

V. We have assigned n_A to the overlapping ideality factors of CuPc/C_{60} and SubPc/C_{60} for reasons discussed below. In Fig. 5(b), the quantity $n\ln(J_s)$ shows a nonlinear Arrhenius dependence in all cases, where the trend is also similar to that predicted in Fig. 2(b).

Figure 6(a) shows the intensity dependence of V_{oc} under simulated AM1.5G solar illumination. Lines are calculated using Eq. (18) along with the ideality factors and dark saturation currents determined from data in Fig. 5. The photocurrent, $q\eta_{PPd}J_X$, is approximated by the short-circuit current density, J_{sc}, measured at each intensity. The slopes are dominated by $n_A k_b T/q$ for both CuPc/C_{60} and SubPc/C_{60} devices; that of $n_D k_b T/q$ only becomes evident at lower intensity.

The temperature dependence of V_{oc} under $\lambda=496$ nm laser illumination is shown in Fig. 6(b). The solid lines are also calculated from Eq. (18) using the temperature dependent n and J_s from Fig. 5 with the photocurrent term given by J_{sc} measured at $T=300$ K. Since the diode parameters characterize the dark current temperature dependence, we infer that the deviation at low temperature is due to a decrease in the polaron pair dissociation efficiency, η_{PPd}. The ratio, $\eta_{PPd}(T)/\eta_{PPd}(300\ \mathrm{K})$, calculated from this difference, is also shown in Fig. 6(b) (dashed lines) and drops by a factor of ~40 between room temperature and $T=114$ K.

In Fig. 7(a), we calculate the normalized power efficiency, η_p, along with V_{oc}, J_{sc}, and FF as a function of the polaron pair recombination rate using the model as in Figs. 2 and 3. Current-voltage characteristics corresponding to several values of k_{PPr} are shown in Fig. 7(b). All of the cell efficiency parameters decrease with increasing recombination rate, and the power-conversion efficiency drops most steeply for $k_{PPr}>1\ \mu s^{-1}$. In contrast, Fig. 8(a) shows the J-V dependence on built-in potential, V_{bi}, for the same model as in Fig. 7(b), with $k_{PPr}=(20\ \mathrm{ns})^{-1}$. Small V_{bi} result in an "S"-shaped kink as observed in some small molecule and polymer organic solar cells.[33–35]

V. DISCUSSION

The trap-free and trap-limited ideal diode equations derived here [Eqs. (7) and (15), respectively] are similar in form to the Shockley equation but the interpretation of the fitting parameters (ideality factors, saturation current densities) is different due to the different nature of excited states in organic and inorganic semiconductors. In inorganic semiconductors, excitation produces free carriers directly, whereas in organic semiconductors, the result of photon ab-

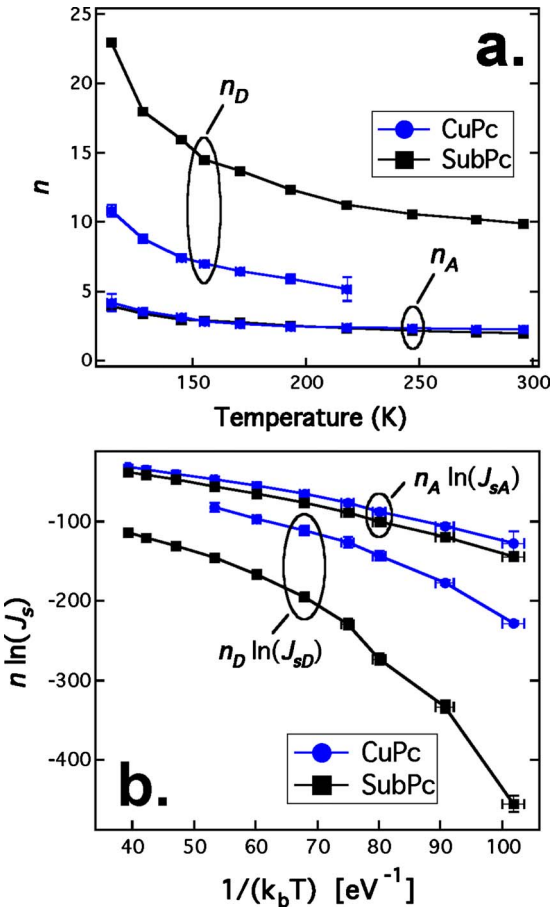

FIG. 5. (Color online) (a) Temperature dependence of the ideality factors derived from the *J-V* data of Fig. 4. The ideality factors increase with decreasing temperature in all cases. Values of n_D and J_{sD} cannot be extracted for CuPc/C_{60} at $T>220$ K because the second exponential term in Eq. (18) is insignificant. (b) Plot of $n \ln(J_s)$ vs $1/k_bT$, where k_bT is the thermal energy, for the CuPc/C_{60} and SubPc/C_{60} devices. Note the similarity in n_A and $n_A \ln(J_{sA})$ between the two cells, which share a common C_{60} acceptor whereas n_D and $n_D \ln(J_{sD})$ clearly differ due to the different donors.

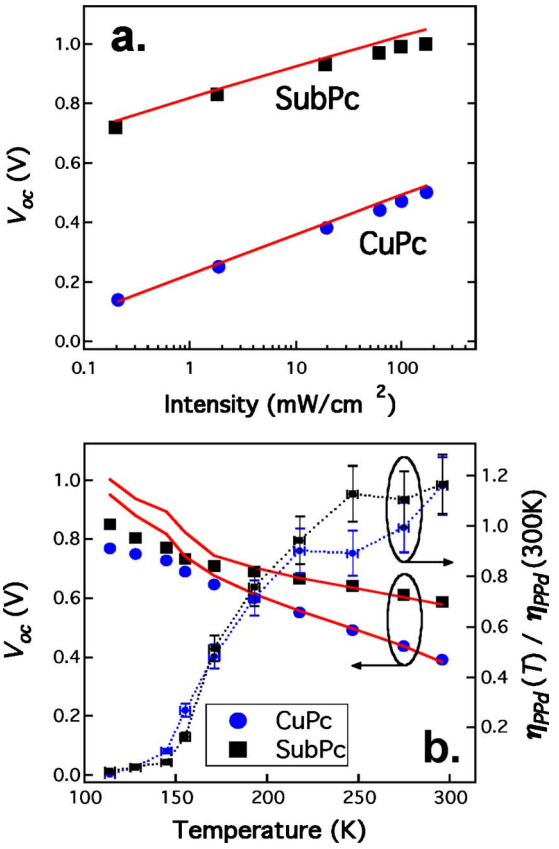

FIG. 6. (Color online) (a) Dependence of the open-circuit voltage, V_{oc}, on the intensity of simulated AM1.5G solar illumination at room temperature. Solid lines are calculated from Eq. (18) using values of n and J_s from Fig. 5 along with the short-circuit current densities measured at each intensity. (b) Temperature dependence of V_{oc} under laser illumination at $\lambda=496$ nm, and at an intensity of 30 mW/cm^2. Solid lines are calculated using the temperature-dependent n and J_s of Fig. 5 and the short-circuit current density measured at room temperature. Deviation between the calculation and the data at low temperature indicates a reduced polaron pair dissociation efficiency, $\eta_{PPd}(T)$, shown on the right-hand axis, and normalized to its value at room temperature. Dashed lines connecting the data points are a guide to the eyes.

sorption is a tightly bound exciton that has a very low probability of dissociating unless charge transfer is initiated at a D-A HJ to form a more loosely bound polaron pair. Thus, in contrast to inorganic *p-n* junctions where current is due to drift diffusion and/or recombination within the depletion region, the current in organic HJs depends on polaron pair recombination and dissociation that occur over a small volume at the HJ interface.

In the absence of shunt paths or other junction defects, generation and recombination via interfacial polaron pairs is the sole source of current flow. This assumption is reasonable at low bias since PPs provide the lowest energy recombination pathway in D-A HJs with type-II (i.e., staggered) HJ energy-level offsets, and hence should be the most heavily populated state at small quasi-Fermi-level separations. As shown in paper II, this is not the case at high bias ($V_a > 2$ V), where both SubPc and C_{60} fluorescence are detected, indicating injection beyond the HJ (i.e., of holes into the acceptor bulk and electrons into the donor) with subsequent exciton formation and recombination in each of the layers. This assumption thus does not apply to organic light-emitting devices, which generally operate at high bias ($V_a > 2$ V) and are designed to minimize energy-level offsets to maximize injection into and exciton formation in the emissive layer bulk.

As in the Shockley equation, we have assumed quasiequilibrium conditions, implying that J is negligible compared to either of its drift or diffusion components. This assumption is rigorous at low currents, but breaks down for $J > 0.1$ A/cm^2, where the voltage drop due to contact and bulk series resistance becomes significant. Space charge effects may also become significant at high currents but are neglected here for simplicity. Beyond these assumptions, the trap-free current-voltage relationship and its consequences for V_{oc} established by Eqs. (9) and (10) are of general validity.

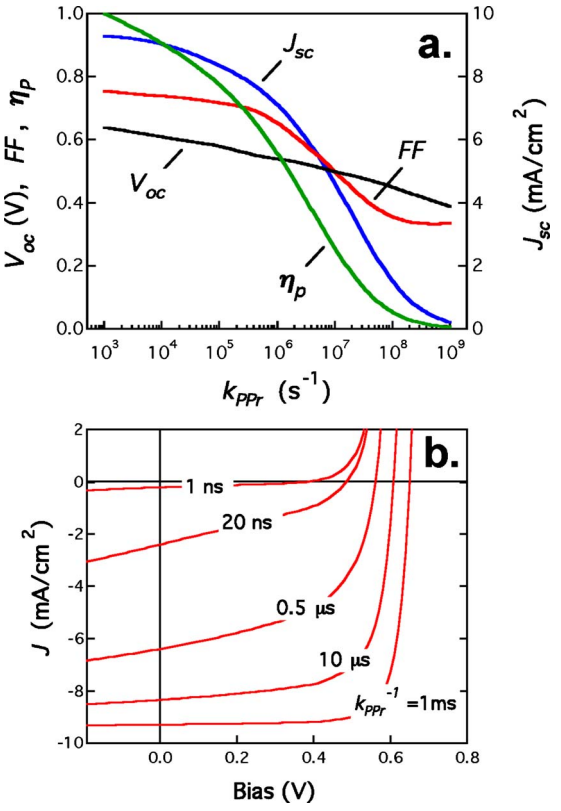

FIG. 7. (Color online) (a) Dependence of open-circuit voltage, fill factor, and short-circuit current (V_{oc}, FF, J_{sc}, respectively), and normalized power-conversion efficiency, η_P, on the polaron pair recombination rate, k_{PPr}. An exciton current of $qJ_X=10$ mA/cm^2 is assumed. (b) Fourth quadrant J-V characteristics at several values of k_{PPr} resulting in the trends shown in (a).

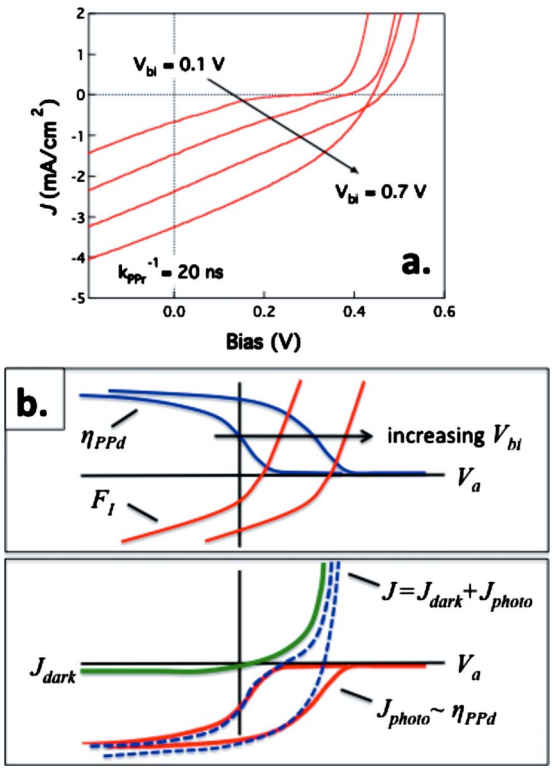

FIG. 8. (Color online) (a) Current-voltage characteristics calculated for V_{bi} ranging from 0.1 to 0.7 V in 0.2 V increments using the same model as in Fig. 7(b) with $k_{PPr}=(20\ \text{ns})^{-1}$. (b) Schematic illustrating the physical basis for the S-kink observed in (a). The top panel shows the dependence of the internal field, F_I, and polaron pair dissociation efficiency, η_{PPd}, on the applied bias, V_a. Dissociation is aided by $F_I<0$. The lower panel shows the corresponding photocurrents, which sum with the dark current to give the total current (dashed lines). When V_{bi} is small, the internal field reaches zero at small V_a, resulting in a rapid change in photocurrent before the dark current becomes appreciable, leading to the S-kink as shown.

Disorder-induced and other trap states complicate the trap-free picture, as the recombination kinetics depend on the particular trap distribution chosen. Regardless of this choice, the double exponential form of the J-V relation given by Eq. (15) is a general result, as it stems from the two possible recombination pathways of free electrons with trapped holes, and vice versa.

Shockley-Hall-Read (SHR) theory provides an alternate way to describe trap-limited recombination.[7] Although this approach has previously been applied to organic solar cells,[15,36] it assumes detailed balance of traps active for both carrier types in a *single* material. In contrast, the organic HJ involves two different sets of traps, active for holes and electrons in the donor and acceptor layers, respectively. The Langevin bimolecular approach of Eq. (12) is well established for organic semiconductors,[11,12] and its application here is more appropriate than the SHR approach.

The fits of Fig. 4 demonstrate that Eq. (18) is an accurate description of the J-V characteristics, as compared to the generalized Shockley equation for CuPc/C_{60} and SubPc/C_{60} solar cells. In Fig. 5, the similarity in n_A and $n_A \ln(J_{sA})$ between CuPc/C_{60} and SubPc/C_{60} suggests that the current component involving these terms is due to recombination with trapped electrons in the C_{60} acceptor common to both HJs. Analogously, the differing n_D and $n_D \ln(J_{sD})$ suggests recombination with trapped holes occupying the different density of states characteristic of CuPc and SubPc.

The values of n and J_s from Fig. 5 give rise to the intensity and temperature dependencies of V_{oc} in Fig. 6. Only one slope is evident in Fig. 6(a) for each device. We expect a second slope, as predicted in Fig. 3(a) to become apparent at low intensity or low temperature. In Fig. 6(b), the deviation in calculated V_{oc} from the data at low temperature is due to the drop in polaron pair dissociation efficiency, as expected from the Onsager-Braun model[10,11] and replicated in Fig. 3(b).

The theoretical and experimental ideality factors [as shown in Figs. 2(b) and 5, respectively] all increase superlinearly with decreasing temperature. However, the experimental values are roughly a factor of 3–4 times larger than predicted and, in the case of n_A, the predicted change is much less than that observed. The magnitude of the change in ideality factor with temperature is strongly dependent on the particular combination of trap temperature/distribution type, and the potential distribution in the device [see Eq. (14)]. The difference in n_A is partially attributed to the particular C_{60} trap distribution that, in contrast to the exponen-

tial distribution of CuPc,[37] is known to develop both shallow and discrete levels even in the presence of minute ambient concentrations of O_2 and H_2O.[38]

Additionally, since δ_D and δ_A do not cancel as in the trap-free case, changes in the potential distribution across the D and A layers with bias and/or temperature will influence the ideality factors. For example, an increase in the potential dropped across the acceptor with decreasing temperature would lead to a correspondingly greater increase in n_A over the same interval. This remains a difficulty for the exponential-trap model, so we emphasize that its primary predictions are two ideality factors that increase superlinearly with decreasing temperature.

The discrepancy in magnitude between the theoretical and observed ideality factors is attributed to our implicit use of the conventional Einstein relation, which may not be appropriate for disordered semiconductors.[19,39] Indeed, the generalized Einstein relation can be written $D/\mu=(k_bT/q)\eta$, where D is the diffusivity and the enhancement factor, η, depends on the particular density of states or trap distribution function. The ideality factors scale in direct proportion to η and in the case of an exponential trap distribution, $\eta \approx T_t/T$.[40] Hence, for $T_t=1000$ K assumed in Table II, the 3–4 times discrepancy in magnitude is accounted for when the generalized Einstein relation is employed.

Previously, V_{oc} was observed to saturate at $T \sim 175$ K for a number of different HJs,[3,5] whereas other recent reports[16,30] and our data in Fig. 6(b) show a monotonic increase with decreasing temperature. The reason for this discrepancy might lie in the difficulty of accurately measuring device temperature under illumination on a thermally insulating glass substrate. A plateau in V_{oc} at intermediate temperature is not predicted in Fig. 3(b) using the parameters in Table II. However, in some asymmetric HJs with different D and A layer thicknesses, trap temperatures, and injection barriers (i.e., ϕ_a and ϕ_c), a plateau is found to emerge between $T=100$ and 150 K.

As shown in Fig. 7, the solar power conversion efficiency depends critically on the polaron pair recombination rate, k_{PPr}. The decline in J_{sc} is due to the decrease in PP dissociation efficiency with increasing k_{PPr}, and the drop in V_{oc} follows Eq. (9). Physically, k_{PPr} describes either the direct recombination of the D^+-A^- charge transfer state, or its indirect recombination, e.g., via a lower-lying triplet state. Estimates for this parameter generally range between 1 ns^{-1} and 1 μs^{-1}, as supported by polaron transient absorption kinetics,[41] electronic modeling of D-A excited states,[42] and Monte Carlo simulations of geminate recombination.[43]

Finally, the "S-kink" behavior found in many organic HJ cells[33–35] in Fig. 8(a) is explained schematically in Fig. 8(b). The top panel illustrates the shift in zero crossing of the internal field ($F_I<0$ favors dissociation) toward positive applied bias with increasing V_{bi}. It leads to a similar shift in the PP dissociation efficiency, η_{PPd}, and hence to a concomitant shift in the photocurrent [cf. Eq. (7)].

The lower panel shows that the total current is the sum of the dark and photocurrents. The S-kink appears when the slope of the photocurrent, as determined by η_{PPd}, is large in the fourth quadrant at low bias, and when the dark current is not yet significant. At room temperature, this typically occurs for a combination of large k_{PPr} (e.g., $\geq 10^7$ s^{-1}) and small V_{bi} (e.g., ≤ 0.3 V). In contrast, at low temperature this feature emerges for a much broader range of V_{bi} and k_{PPr}, since under these conditions, k_{PPd} is small, shifting the η_{PPd} curve (see top panel) toward low applied bias. An S-kink is thus expected to be a general feature in the J-V characteristic of organic HJ solar cells under illumination at low temperature.

Understanding and minimizing the PP recombination rate is clearly important for achieving high-efficiency organic solar cells. The k_{PPr} employed in the Onsager-Braun model may, in fact, be the result of multiple recombination pathways, potentially involving intermediate states, and depending on such factors as mutual orientation and orbital overlap between the donor and acceptor molecules at the heterointerface. For example, Perez *et al.* linked the degree of π-π overlap and intermolecular interaction between the donor and acceptor to the dark saturation current and V_{oc} in a broad selection of molecules.[24] Both of these factors depend directly on the magnitude of k_{PPr}. Additionally, rapid intersystem crossing between singlet and triplet PP configurations due to the small exchange splitting can make recombination via a triplet exciton favorable if such a state exists below the PP energy.[41,44] Further investigation into the nature of k_{PPr} at CuPc/C_{60} and SubPc/C_{60} HJs is the subject of paper II.[8]

Finally, we note that the double exponential current-voltage characteristic is not unique to organic heterojunctions but is rather a general result that follows whenever two recombination pathways of different order exist at a junction. For example, in inorganic p-n junctions, one often observes a transition from sub-linear, trap-limited recombination in the depletion region at low bias (ideality $n \sim 2$) to drift/diffusion current at higher bias (ideality $n=1$), where "drift/diffusion" is recognized simply as linear recombination in the quasineutral bulk.[7,45] Ideality factors >2 result from recombination that accompanies broad, continuous trap distributions, and hence are most often observed for amorphous organic and inorganic (i.e., a-Si:H) junctions.[46]

VI. CONCLUSION

We have derived an analytical model that describes the current-voltage characteristics of organic heterojunctions. The model is based on polaron pair generation and recombination processes at the donor-acceptor interface and leads to an ideal diode equation that is demonstrated for small molecule organic planar heterojunctions. These results should also be generally applicable to polymer and small molecule bulk heterojunctions, although the required electrostatic calculations are more complicated in this latter case owing to the increased dimensionality of the junction.

In particular, the dark current is shown to be directly proportional to the polaron pair recombination rate, and the open-circuit voltage is ultimately limited by the difference between the donor-acceptor interface energy gap and the polaron pair binding energy, as observed previously.[5,16]

We propose that recombination at traps within the disorder-induced density of states tail in each material at the D-A heterointerface results in two, temperature-dependent ideality factors, and a commonly observed double exponen-

tial *J-V* characteristic. Using an exponential trap distribution, we have reproduced the trends observed for the dark current, V_{oc}, and J_{sc} as a function of temperature and intensity.

Our results lead to the following interpretation of the current vs voltage characteristics. (1) The reverse-bias slope of the dark current reflects the increasing dissociation probability of thermally generated PPs at the HJ. (2) In forward bias, there are two exponential regions, each with its own ideality factor stemming from recombination with trapped/immobile carriers at each side of the HJ. (3) The ideality factors are interpreted as the extent to which trap-limited recombination (one free and one immobile carrier) dominates over free carrier recombination (both carriers mobile). (4) The ratio of the two exponential current components under forward bias reflects the relative contribution of free donor holes recombining with trapped acceptor electrons vs the reverse process to the total current density. (5) Large ideality factors (>2) are due to a broad trap DOS distribution and/or large asymmetries in the potential dropped across the donor and acceptor layers. (6) Both ideality factors increase with decreasing temperature as more carriers freeze into the DOS tail and trap-limited recombination increases.

We have identified the polaron pair recombination rate as a critical parameter for cell efficiency that is poorly characterized to date. In paper II,[8] we directly investigate the nature of this process for the organic HJs studied here.

ACKNOWLEDGMENTS

This work was supported in part by Department of Energy, Office of Basic Energy Sciences as part of Energy Frontier Research Centers: the Center for Solar and Thermal Energy Conversion at the University of Michigan (Award No. DE-SC0000957, S.R.F.) and the Argonne-Northwestern Solar Energy Research (ANSER) Center (Contract No. DE-SC0001059, N.C.G., G.P.W., and M.R.W.). The Center for Nanoscale Materials is funded by the U.S. Department of Energy, Office of Science, Office of Basic Energy Sciences under Contract No. DE-AC02-06CH11357 (N.C.G., G.P.W., and M.R.W.). We also thank B. E. Lassiter (supported by the Air Force Office of Scientific Research and Global Photonic Energy Corp.) for technical assistance.

APPENDIX: CALCULATION OF THE INTERFACIAL ELECTRIC FIELD

The interfacial electric field is required to calculate the polaron pair dissociation efficiency, $\eta_{\mathrm{PP}d}$, in Eqs. (7) and (15). Assuming that free carriers determine the potential distributions in their respective layers (e.g., holes (p) in the donor and electrons (n) in the acceptor), then in quasiequilibrium, $p\mu F \approx Dp'(x)$, and the Poisson equation gives $FF' - (D/\mu)F'' = 0$.[15] Here, D is the diffusion coefficient, μ is the mobility of the charge under consideration, and F is the electric field. Assuming the Einstein relation between D and μ and defining $\beta = q/k_bT$, these equations may be solved as in Ref. 32 or they may be integrated once and solved as a Riccati equation.[47] Defining the constant $C_1 = F_I^2 - 2qp_I/(\beta\varepsilon)$, we obtain

$$F(x) = \left[\frac{1}{F_I} - \frac{\beta x}{2}\right]^{-1}, \tag{A1a}$$

$$p(x) = \frac{\beta\varepsilon}{2q}\left[\frac{1}{F_I} - \frac{\beta x}{2}\right]^{-2} \tag{A1b}$$

when $C_1 = 0$ and

$$F(x) = \sqrt{C_1}\left[1 + \frac{2(F_I - \sqrt{C_1})}{(F_I + \sqrt{C_1})\exp(-\sqrt{C_1}\beta x) - (F_I - \sqrt{C_1})}\right], \tag{A2a}$$

$$p(x) = \frac{2\beta\varepsilon}{q} C_1 \exp(\sqrt{C_1}\beta x) \times \frac{(F_I - \sqrt{C_1})(F_I + \sqrt{C_1})}{[(F_I + \sqrt{C_1}) - (F_I - \sqrt{C_1})\exp(\sqrt{C_1}\beta x)]^2} \tag{A2b}$$

when $C_1 \neq 0$, for both positive and negative values of C_1. As in the text, F_I and p_I are the electric field and hole density at the donor-acceptor interface located at position $x=0$. Since both the hole density at the interface and at the contact ($x = x_C$) are known from Eqs. (4) and (6), Eq. (A2b) can be solved implicitly for F_I.

For the case of an exponential trap distribution, where we assume $p_t \gg p$, trapped carriers dominate the field distribution and the Poisson equation is $F' \approx qp_t/\varepsilon$. Since quasiequilibrium maintains for free carriers, the analog of Eq. (11) for holes is used to obtain $FF' - (Dl_{\mathrm{D}}/\mu)F'' = 0$. Thus, Eqs. (A1) and (A2) remain valid upon substituting $\beta \rightarrow \beta/l_{\mathrm{D}}$, where Eq. (A2b) now refers to the *trapped* hole density. Using Eq. (11) to relate the trapped ($p_{C,t}$) and free (p_C) hole densities at the anode, with the latter given by Eq. (6), we use $p_{It} = p_{C,t}\exp[-q\delta_{\mathrm{D}}(V_a - V_{bi})/l_{\mathrm{D}}k_bT]$ and Eq. (A2b) to again solve for F_I.

After determining F_I, the polaron pair dissociation efficiency is calculated using the Onsager-Braun model,[10] which we summarize here. Given an initial PP separation, a_0, the dissociation rate $k_{\mathrm{PP}d}$ is

$$k_{\mathrm{PP}d} = \frac{3}{4\pi a_0^3} k_{rec} \exp(-E_B/k_bT)\frac{J_1[2\sqrt{-2b}]}{\sqrt{-2b}}, \tag{A3}$$

where $b = q^3F_I/(8\pi\varepsilon k_b^2T^2)$ and J_1 is the Bessel function of order 1. To account for disorder, we take a range of initial separations according to the normalized distribution function[13] $f(x) = 4/(\sqrt{\pi}a_0^3)x^2\exp(-x^2/a_0^2)$ and integrate it over the entire current density expression, since $k_{\mathrm{PP}d}$ appears independently in addition to $\eta_{\mathrm{PP}d}$.

The validity of Eq. (A3) for negative fields (i.e., when F_I reverses direction under sufficient forward bias) is unclear, and its numerical evaluation becomes unstable for $F_I < -10^4$ V/cm. Analogy to the Onsager theory suggests[11] that $k_{\mathrm{PP}d}$ retains it zero field value at $F_I < 0$, however, this discontinuity seems unphysical, and Monte Carlo simulations show

that the dissociation efficiency at a D-A heterojunction does indeed decrease for fields directed toward the HJ.[48] Thus, when $F_I<0$, we take the zero field $k_{\mathrm{PP}d}$ and augment the PP binding energy with the additional barrier $-qF_I r_c \cos\theta$, where $r_c=q^2/(4\pi\varepsilon k_b T)$ is the Onsager radius.[11] We then average over the forward half space of angles $-\pi/2<\theta<\pi/2$ between the PP separation vector and the HJ normal to account for the distribution of initial PP orientations.[48]

*stevefor@umich.edu

[1] W. Shockley, Bell System Tech. J. **28**, 435 (1949).
[2] W. Shockley, *Electrons and Holes in Semiconductors with Applications to Transistor Electronics* (D. Van Nostrand, New York, 1950).
[3] V. Dyakonov, Appl. Phys. A: Mater. Sci. Process. **79**, 21 (2004).
[4] W. J. Potscavage, S. Yoo, and B. Kippelen, Appl. Phys. Lett. **93**, 193308 (2008).
[5] B. P. Rand, D. P. Burk, and S. R. Forrest, Phys. Rev. B **75**, 115327 (2007).
[6] N. Li, B. E. Lassiter, R. R. Lunt, G. Wei, and S. R. Forrest, Appl. Phys. Lett. **94**, 023307 (2009).
[7] S. M. Sze, *Physics of Semiconductor Devices* (Wiley, New York, 2005).
[8] N. C. Giebink, B. E. Lassiter, G. P. Wiederrecht, M. R. Wasielewski, and S. R. Forrest, following paper, Phys. Rev. B **82**, 155306 (2010).
[9] T. Kirchartz, B. E. Pieters, K. Taretto, and U. Rau, J. Appl. Phys. **104**, 094513 (2008).
[10] C. L. Braun, J. Chem. Phys. **80**, 4157 (1984).
[11] M. Pope and C. E. Swenberg, *Electronic Processes in Organic Crystals and Polymers* (Oxford University Press, New York, 1999).
[12] C. Groves and N. C. Greenham, Phys. Rev. B **78**, 155205 (2008).
[13] V. D. Mihailetchi, L. J. A. Koster, J. C. Hummelen, and P. W. M. Blom, Phys. Rev. Lett. **93**, 216601 (2004).
[14] J. C. Scott and G. G. Malliaras, Chem. Phys. Lett. **299**, 115 (1999).
[15] D. Cheyns, J. Poortmans, P. Heremans, C. Deibel, S. Verlaak, B. P. Rand, and J. Genoe, Phys. Rev. B **77**, 165332 (2008).
[16] K. Vandewal, K. Tvingstedt, A. Gadisa, O. Inganas, and J. V. Manca, Phys. Rev. B **81**, 125204 (2010).
[17] W. Shockley and H. J. Queisser, J. Appl. Phys. **32**, 510 (1961).
[18] H. Bässler, Phys. Status Solidi B **175**, 15 (1993).
[19] N. Tessler, Y. Preezant, N. Rappaport, and Y. Roichman, Adv. Mater. **21**, 2741 (2009).
[20] P. E. Burrows, Z. Shen, V. Bulovic, D. M. McCarty, S. R. Forrest, J. A. Cronin, and M. E. Thompson, J. Appl. Phys. **79**, 7991 (1996).
[21] P. Sreearunothai, A. C. Morteani, I. Avilov, J. Cornil, D. Beljonne, R. H. Friend, R. T. Phillips, C. Silva, and L. M. Herz, Phys. Rev. Lett. **96**, 117403 (2006).
[22] C. Groves, J. C. Blakesley, and N. C. Greenham, Nano Lett. **10**, 1063 (2010).
[23] K. C. Kao and W. Hwang, *Electrical Transport in Solids* (Pergamon Press, Oxford, 1981).
[24] M. D. Perez, C. Borek, S. R. Forrest, and M. E. Thompson, J. Am. Chem. Soc. **131**, 9281 (2009).
[25] E. Tutiš, D. Berner, and L. Zuppiroli, J. Appl. Phys. **93**, 4594 (2003).
[26] S. J. Martin, G. L. B. Verschoor, M. A. Webster, and A. B. Walker, Org. Electron. **3**, 129 (2002).
[27] R. A. Marsh, C. R. McNeill, A. Abrusci, A. R. Campbell, and R. H. Friend, Nano Lett. **8**, 1393 (2008).
[28] L. J. A. Koster, V. D. Mihailetchi, R. Ramaker, and P. W. M. Blom, Appl. Phys. Lett. **86**, 123509 (2005).
[29] L. J. A. Koster, V. D. Mihailetchi, H. Xie, and P. W. M. Blom, Appl. Phys. Lett. **87**, 203502 (2005).
[30] H. Kumar, P. Kumar, N. Chaudhary, R. Bhardwaj, S. Chand, S. C. Jain, and V. Kumar, J. Phys. D **42**, 015102 (2009).
[31] V. Dyakonov, Thin Solid Films **451**, 493 (2004).
[32] K. L. Mutolo, E. I. Mayo, B. P. Rand, S. R. Forrest, and M. E. Thompson, J. Am. Chem. Soc. **128**, 8108 (2006).
[33] A. Kumar, S. Sista, and Y. Yang, J. Appl. Phys. **105**, 094512 (2009).
[34] D. Gupta, M. Bag, and K. S. Narayana, Appl. Phys. Lett. **92**, 093301 (2008).
[35] A. Geiser, B. Fan, H. Benmansour, F. Castro, J. Heier, B. Keller, K. E. Mayerhofer, F. Nuesch, and R. Hany, Sol. Energy Mater. Sol. Cells **92**, 464 (2008).
[36] M. M. Mandoc, F. B. Kooistra, J. C. Hummelen, B. de Boer, and P. W. M. Blom, Appl. Phys. Lett. **91**, 263505 (2007).
[37] K. Celebi, P. J. Jadhav, K. M. Milaninia, M. Bora, and M. A. Baldo, Appl. Phys. Lett. **93**, 083308 (2008).
[38] T. Matsushima, M. Yahiro, and C. Adachi, Appl. Phys. Lett. **91**, 103505 (2007).
[39] Y. Roichman and N. Tessler, Appl. Phys. Lett. **80**, 1948 (2002).
[40] N. Tessler and Y. Roichman, Org. Electron. **6**, 200 (2005).
[41] S. Westenhoff, I. A. Howard, J. M. Hodgkiss, K. R. Kirov, H. A. Bronstein, C. K. Williams, N. C. Greenham, and R. H. Friend, J. Am. Chem. Soc. **130**, 13653 (2008).
[42] Y. S. Huang, S. Westenhoff, I. Avilov, P. Sreearunothai, J. M. Hodgkiss, C. Deleener, R. H. Friend, and D. Beljonne, Nature Mater. **7**, 483 (2008).
[43] C. Deibel, T. Strobel, and V. Dyakonov, Phys. Rev. Lett. **103**, 036402 (2009).
[44] D. Veldman, S. C. J. Meskers, and R. A. J. Janssen, Adv. Funct. Mater. **19**, 1939 (2009).
[45] J. Nelson, *The Physics of Solar Cells* (Imperial College Press, London, 2003).
[46] J. Pallares, R. Cabre, L. F. Marsal, and R. E. Schropp, J. Appl. Phys. **100**, 084513 (2006).
[47] C. M. Bender and S. A. Orszag, *Advanced Mathematical Methods for Scientists and Engineers* (McGraw-Hill, New York, 1978).
[48] P. Peumans and S. R. Forrest, Chem. Phys. Lett. **398**, 27 (2004).